frontiers | Frontiers in Earth Science

ORIGINAL RESEARCH
published: 11 April 2022
doi: 10.3389/feart.2022.855879

Coupling Relationship Between Densification Characteristics and Tight Oil Accumulation of the FGSR Reservoir: A Case Study of the Chang 7 Member of the Triassic Yanchang Formation in the Zhenyuan Area of the Southwest Ordos Basin, Central China

Weiling He[1,2]*, *Ruyue Wang*[1,2]*, *Qiqi Lyu*[3,4], *Jun Liu*[5] and *You Wu*[3,4]

[1]SINOPEC Petroleum Exploration and Production Research Institute, Beijing, China, [2]State Key Laboratory of Shale Oil and Gas Enrichment Mechanisms and Effective Development, Beijing, China, [3]School of Geosciences, Yangtze University, Wuhan, China, [4]Hubei Cooperative Innovation Center of Unconventional Oil and Gas (Yangtze University), Wuhan, China, [5]Gas Field Development Department, PetroChina Changqing Oilfield Company, Xi'an, China

OPEN ACCESS

Edited by:
Kun Zhang,
Southwest Petroleum University, China

Reviewed by:
Jianhua He,
Chengdu University of Technology, China
Zhonghu Wu,
Guizhou University, China
Qilu Xu,
China University of Petroleum, China

***Correspondence:**
Weiling He
halahwl@163.com
Ruyue Wang
wry1990@vip.qq.com

Specialty section:
This article was submitted to Geochemistry, a section of the journal Frontiers in Earth Science

Received: 16 January 2022
Accepted: 25 February 2022
Published: 11 April 2022

Citation:
He W, Wang R, Lyu Q, Liu J and Wu Y (2022) Coupling Relationship Between Densification Characteristics and Tight Oil Accumulation of the FGSR Reservoir: A Case Study of the Chang 7 Member of the Triassic Yanchang Formation in the Zhenyuan Area of the Southwest Ordos Basin, Central China. Front. Earth Sci. 10:855879. doi: 10.3389/feart.2022.855879

Fine-grained sedimentary rock (FGSR) reservoirs in a deep-water sedimentary environment from the Late Triassic Yanchang Formation in the Ordos Basin in central China have huge potential for tight oil production. According to the comprehensive research of fluid inclusion experiment, scanning electron microscopy, cathodoluminescence, thin section identification, and whole rock analysis, the petrographic characteristics, fluorescence spectrum parameters, and the homogenization temperature of oil inclusions and associated brine inclusions in the FGSR reservoir were analyzed to explore the coupling relationship between densification characteristics and tight oil accumulation of the FGSR reservoir. The results show the FGSR reservoir diagenesis has experienced compaction, cementation, and multiple stages of dissolution. A comprehensive analysis of burial history shows that the Chang 7 Member FGSR reservoir in the study area has three phases of oil charging, corresponding to the geologic time range of 132–124, 120–102, and 98–97 Ma. The organic acid produced by the first-stage oil charging accelerated the dissolution of feldspar and cuttings, and the dissolution pores increased significantly. Then, the organic acid in the second-stage oil charging accelerated the dissolution, and the abnormally high hydrocarbon expulsion pressure inhibited the damage of compaction on the pores of FGSR reservoir. Finally, the thermal evolution degree of source rocks reached the highest in the third-stage oil charging. The constructive effect of large-scale organic acids on pores and the protective effect of the chlorite membrane on pores inhibited the densification process of the FGSR reservoir. In short, the FGSR reservoir has experienced a cyclical reservoir densification process of "reducing porosity–increasing porosity–preserving porosity." The coupling of pore evolution and oil charging of the FGSR reservoir is the key to the extensive accumulation and large-scale reservoir formation

of tight oil in the Chang 7 Member of the Yanchang Formation in the Zhenyuan area, southwest Ordos Basin. The significance of the study may help to understand the process of the tight oil accumulation and predict the tight oil of the FGSR reservoir distribution.

Keywords: fine-grained sedimentary rocks, fluid inclusion, diagenesis, Yanchang Formation, Ordos Basin

INTRODUCTION

Unconventional oil and gas exploration in the Bakken Formation in the Willingston Basin, Eagle Ford Formation in southern Texas, and Barnett Formation in the Fort Worth Basin in north-central Texas in North America achieved significant success (Loucks et al., 2009; Sonnenberg and Pramudito, 2009), showing that the unconventional resources represented by shale gas and tight oil have become a new frontier for global oil and gas exploration and development. In China, unconventional oil and gas are widespread in the FGSRs of several large hydrocarbon-containing reservoir basins, such as the Cretaceous Qingshankou Formation of the Songliao Basin (Li et al., 2017), Jurassic Daanzhai Member and the upper Ordovician-lower Silurian Wufeng-Longmaxi in the Sichuan Basin (Wang et al., 2019; Wang et al., 2020; Wang et al., 2021; Zhang et al., 2022), and Chang 7 Member of the Triassic Yanchang Formation in the Ordos Basin (Yao et al., 2013; Yang et al., 2017), exhibiting huge resource potential (Huang et al., 2018). Among them, the tight oil in the FGSR reservoir in the Chang 7 Member of the Triassic Yanchang Formation in the Ordos Basin in central and western China has achieved rapid exploration breakthroughs. As of the end of 2016, the calculated resources are about 20×10^8 t (Yang et al., 2017). With the discovery of Qingcheng Oilfield with reserves of more than 1 billion tons in September 2019, Changqing Oilfield, PetroChina made substantial breakthroughs in the continuous in-depth study of Chang 7 FGSRs and unconventional oil and gas, which further revealed the huge hydrocarbon generation potential and tight oil accumulation scale in the FGSR reservoir of the Chang 7 Member.

With the continuous tight oil exploration and development in recent years, scholars have made a wealth of knowledge in studying the relationship between densification characteristics and tight oil accumulation of the FGSR reservoir in the Chang 7 Member of the Triassic Yanchang Formation in the Ordos Basin. Some researchers believe that diagenesis plays a decisive role in the densification process of reservoirs (Zhang et al., 2013) in that the remaining pressure difference is the main driving force for tight oil charging when the tight oil has not yet begun to be charged on a large scale before reservoir densification (Guo et al., 2017). In contrast, some believe that when the Triassic Yanchang Formation reaches the peak of hydrocarbon generation and expulsion, the reservoir has not yet been densified and that later, iron carbonate cementation is the decisive factor, leading to the tightness of the reservoir (Deng et al., 2009). Meanwhile, other researchers believe that combined with the analysis of inclusion testing, large-scale mature oil charging has begun before reservoir densification, and the oil charging continued after the formation of tight reservoirs (Zhao et al., 2018). From that given above, it can be seen that the relationship between densification characteristics and tight oil accumulation of the FGSR reservoir is a hot academic topic. The views that the scholars acquired based on relative data are reasonable, but the time sequence and relationship between densification characteristics and tight oil accumulation of the FGSR reservoir are still not clear.

Based on relevant research results, we studied the FGSRs of the Chang 7 Member of the Triassic Yanchang Formation in the Zhenyuan area of the southwest Ordos Basin with a systematic study by comprehensive fluid inclusion analysis, scanning electron microscope microscopic observation, cathode emission analysis, cast thin section and conventional thin section identification, and whole rock analysis. We analyzed the densification process and tight oil charging caused by diagenesis in the FGSR reservoir and provided a theoretical guide in analyzing the unfavorable factors of reservoir densification on tight oil accumulation and in finding favorable tight oil "sweet spot" accumulation areas.

GEOLOGICAL SETTING

Ordos Basin, with a total area of 32×104 km^2, is located to the west of the North China Platform in China, and at the junction of the eastern stability zone and the western active zone. It is the second largest sedimentary basin in China (Yang et al., 2017; Yang et al., 2019). According to its geological evolution history and structural characteristics, the basin can be divided into six primary structural units: Yimeng Uplift, Weibei Uplift, Jinxi Flexfold Belt, Shaanbei Slope, Tianhuan Depression, and the thrust belt on the western edge (Zou et al., 2012; Liao et al., 2013; Li et al., 2016) (**Figure 1A**).

During the depositional period of the Late Triassic Yanchang Formation, the Ordos Basin had extensive water, showing the characteristics of a typical large inland depression lake basin. The western and southern edges of the basin are relatively steep, and the overall slope can reach 3.5°–5.5° (Fu et al., 2010). Due to the sufficient supply of terrigenous clastics at the periphery of the basin, a set of well-developed sedimentary combinations, mainly river delta–lacustrine deposits, was formed during the extended period. They have well-developed sources, reservoirs, and caps with a total thickness of about 100–1,300 m (Yang et al., 2019). The Yanchang Formation can be divided from top to bottom into 10 members from the Chang 1 Member to Chang 10 Member. During the depositional period, it experienced three large lake transgressions in Chang 9, Chang 7, and Chang 4 + 5, wherein the development of lake basin in the Chang 7 Member reached its peak and formed high-quality source rocks (Yang et al., 2010; Yang et al., 2017; Yang et al., 2019) (**Figure 1C**).

The Zhenyuan area with a total area of about 4,500 km^2 is located in southwest Ordos Basin, spanning the southern end of the Tianhuan Depression from east to west, and bordering the

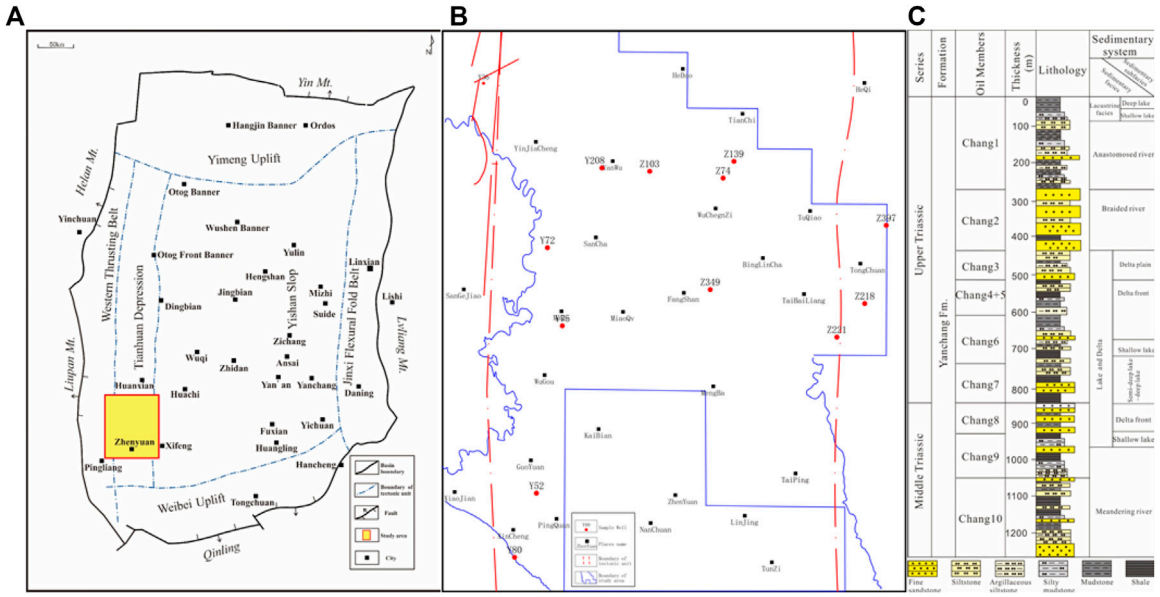

FIGURE 1 | (A) Structural units and geological setting of the Ordos Basin (modified from References Zou et al., 2012 and Li et al., 2016). **(B)** Location of the study area. **(C)** Triassic succession.

thrust belt on the western edge and Yishan Slope to the east (**Figure 1B**). The study area is generally developed on steep slopes, close to the deposition center, which is easy to form slump deposits (Cui et al., 2015). The Chang 7 Member of the Yangchang Formation is mainly a braided river delta–lacustrine sedimentary system, and the semi-deep lake area develops sandy debrite flow and turbidite sedimentary sand body. FGSRs are mainly gray, dark gray, light gray and gray–green fine sandstone and siltstone, dark mudstone, and oil shale (Yuan et al., 2015). The particle diameter range is from 0.03 to 0.60 mm. Evenly sorted and poorly rounded, the particles are mainly sub-angular and sub-round–sub-angular. Through the statistical analysis of quartz, feldspar, and lithic content of 170 sample points, the results show that the rock types are mainly feldspathic lithic sandstone and feldspathic lithic sandstone, followed by lithic feldspar sandstone and lithic sandstone. Among them, feldspathic lithic sandstone and feldspar lithic sandstone account for 68.23% of the total samples, lithic feldspar sandstone 23.53%, and lithic sandstone 8.24%. The feldspar content and lithic content are relatively high. The overall content has relatively low ingredient maturity and relatively high structural maturity. The physical properties of the reservoir are poor, the porosity is generally 6–14%, and the permeability is (0.01–10) × 10^{-3} μm^2, which shows that it is a typical low porosity and low permeability reservoir (Ran et al., 2013).

METHODS

In this study, core samples from 11 key exploratory wells were collected evenly in the Chang 7 Member of the Triassic Yanchang Formation in the Zhenyuan area of the southwest Ordos Basin, and core samples were sorted, screened, and numbered. Among them, there are 20 fluid inclusion samples and 5 scanning electron microscope samples. The sampling well positions are shown in **Figure 1B**. The testing process of the fluid inclusion samples is: sample collection and preparation, diagenesis observation, fluid inclusion microscopic fluorescence observation, oil inclusion microscopic fluorescence spectrum analysis, and fluid inclusion temperature measurement and analysis. In this study, Nikon 80I dual-channel fluorescence microscope was used, and the excitation wavelength of ultraviolet excitation light was 330–380 nm; the fluorescence microscopy spectrometer was Maya 2000 Pro spectrometer of Ocean Optics Inc., and the Leica DM5500 laser fluorescence confocal scanning microscope was used to accurately measure the gas–liquid ratio of inclusions. British Linkam THMS G600 cold/hot stage was used for homogenization temperature and salinity testing of fluid inclusions. Yuanao microscopic spectrum analysis software was used for spectral data processing and graphing. Scanning electron microscope samples were tested with KYKY-3800 scanning electron microscope, and pore throat scanning analysis and diagenesis analysis were performed on the samples. In addition, experimental tests such as cast thin sections, cathodoluminescence, and whole rock analysis were carried out.

RESULTS

Petrographic Characteristics of Hydrocarbon Inclusions

The different fluorescent colors of hydrocarbon inclusions show differences in their composition and maturity. Usually, as the

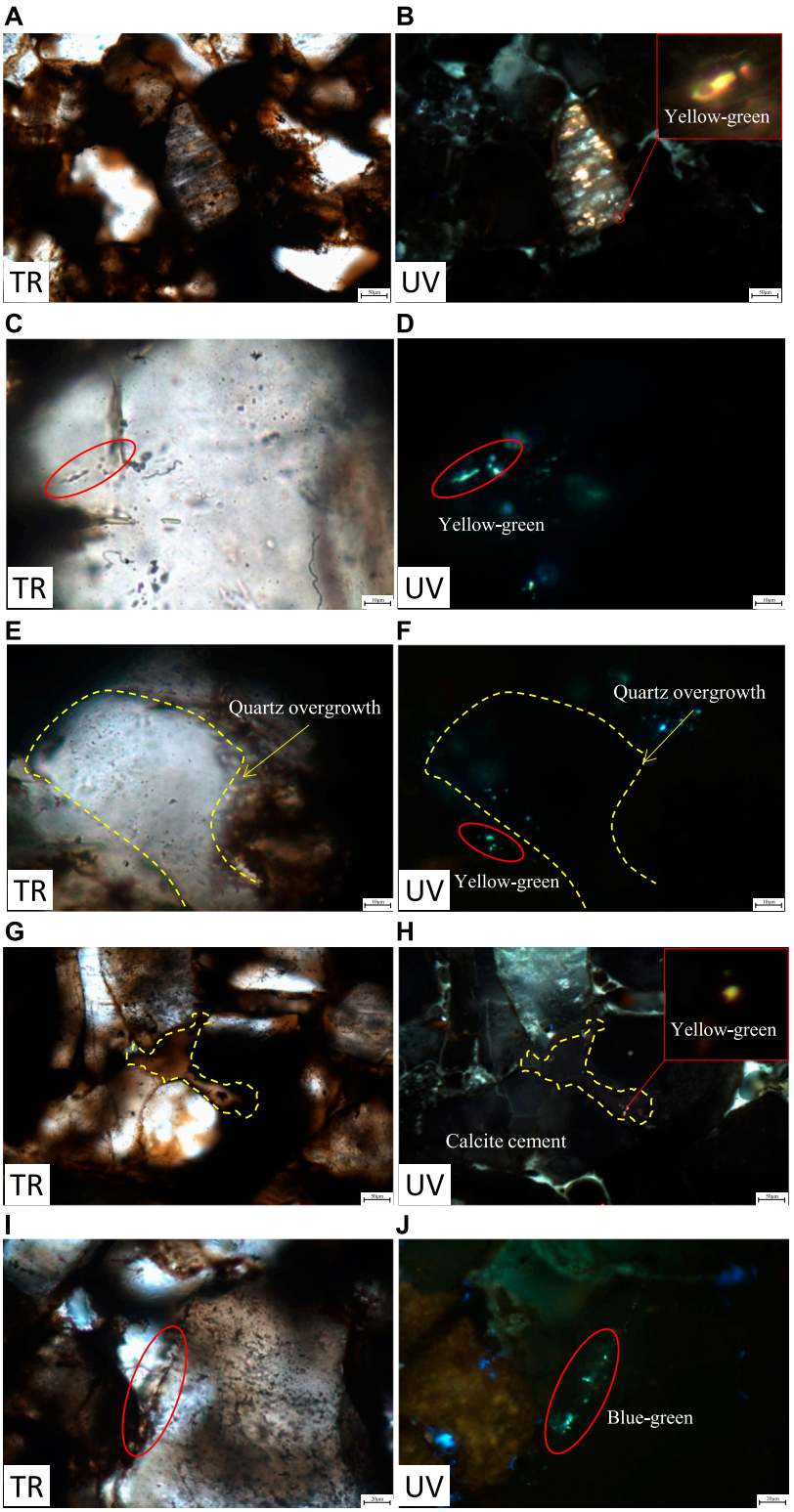

FIGURE 2 | Micrographs of representative oil inclusions under transmitted light (TR) and ultraviolet light (UV) in the FGSR samples. **(A,B)** Sample 2413.48 m, well Y75: yellow–green fluorescing oil inclusions in the dissolved pores of feldspar grains. **(C,D)** Sample 2166 m, well Z218: yellow–green fluorescing oil inclusions along multiple healed fractures of a quartz grain. **(E,F)** Sample 2517.1 m, well Z74: yellow–green fluorescing oil inclusions along healed fractures of quartz overgrowth. **(G,H)** Sample 2360.5 m, well Y75: yellow–green fluorescing oil inclusions in the calcite cement. **(I,J)** Sample 2532.6 m, well Y208: blue–green fluorescing oil inclusions along the fracture through the quartz grain.

TABLE 1 | Microbeam fluorescence color observation and fluorescence spectrum parameters (Q value, λmax value, and QF_{535} value) of oil inclusions with various colors and locations.

Well	Depth/m	Lithology	λ/nm	Q	QF535	Color	Position
Z74	2517.10	Fine sandstone	494.30	0.16	0.75	Blue–green	Healed fracture of quartz grain
			513.78	0.19	0.86	Green	Fracture through the quartz grain
			523.29–528.71	0.27	1.13–1.15	Yellow–green	Quartz overgrowth
							Healed fracture of quartz grain
Z397	2059.03	Siltstone	496.11	0.28	0.94	Blue–green	Calcite cement
			491.57–497.47	0.27–0.28	0.78–0.98	Blue–green	Healed fracture of quartz grain
Z349	2297.37	Siltstone	494.75–497.93	0.20–0.24	0.76–0.84	Blue–green	Fracture through the quartz grain
							Calcite cement
Z221	2063.00	Siltstone	517.40–517.86	0.32–0.33	1.14–1.16	Green	Healed fracture of quartz grain
							Feldspar
Z218	2166.00	Fine sandstone	535.93–544.50	0.38–0.47	1.24–1.38	Yellow–green	Fracture through the quartz grain
							Fracture through the quartz grain
Z139	2589.50	Fine sandstone	518.31	0.31	1.10	Green	Vein
			544.04	0.63	1.86	Yellow–green	Vein
Y52	2143.00	Fine sandstone	459.27–466.56	0.19–0.31	0.60–0.81	Blue	Healed fracture of quartz grain
			487.94–492.48	0.15–0.56	0.61–1.32	Blue–green	Healed fracture of quartz grain
			502.01	0.61	1.48	Green	Healed fracture of quartz grain
Y72	2383.70	Fine sandstone	471.12	0.26	0.83	Blue	Fracture through the quartz grain
	2385.70		523.28–548.55	0.41–0.60	1.23–1.73	Yellow–green	Healed fracture of quartz grain
	2383.70						Quartz overgrowth
							Feldspar
							Feldspar
	2385.70						Feldspar
							Feldspar
	2385.70						Healed fracture of quartz grain
	2383.70						Fracture through the quartz grain
	2385.70						Fracture through the quartz grain
Y75	2413.48	Siltstone	497.02	0.26	0.89	Blue–green	Fracture through the quartz grain
	2448.16	Siltstone					Fracture through the quartz grain
							Fracture through the quartz grain
							Fracture through the quartz grain
	2360.50	Fine sandstone	509.26–513.33	0.27–0.75	0.92–1.77	Green	Healed fracture of quartz grain
							Fracture through the quartz grain
	2413.48	Siltstone	520.57–547.20	0.38–0.44	1.22–1.50	Yellow–green	Fracture through the quartz grain
							Feldspar
			582.25	0.98	2.85	Yellow	Healed fracture of quartz grain
Y80	2209.98	Fine sandstone	463	0.16–0.30	0.64–1.02	Blue	Fracture through the quartz grain
			463.37–499.29	0.16–0.30	0.64–1.02	Blue–green	Fracture through the quartz grain
	2213.40						Fracture through the quartz grain
							Fracture through the quartz grain
							Fracture through the quartz grain
Y208	2492.50	Fine sandstone	487.03–497.02	0.16–0.39	0.65–1.16	Blue–green	Healed fracture of quartz grain
							Healed fracture of quartz grain
	2509.80	Fine sandstone					Fracture through the quartz grain
							quartz overgrowth
	2532.60	Siltstone					Fracture through the quartz grain
	2486.40	Siltstone	533.67–542.69	0.41–0.63	1.38–1.71	Yellow–green	Fracture through the quartz grain
	2509.80	Fine sandstone					Calcite cement
							Feldspar
							Healed fracture of quartz grain

maturity of hydrocarbons increases, their fluorescent colors will evolve in accordance with the red–orange–yellow–green–blue change rule. Therefore, by observing the fluorescence color, fluorescence intensity, and fluorescence spectrum parameters (Q value, λ_{max} value, and QF535 value) of oil inclusions under a microscope, we conducted an indirect analysis of the

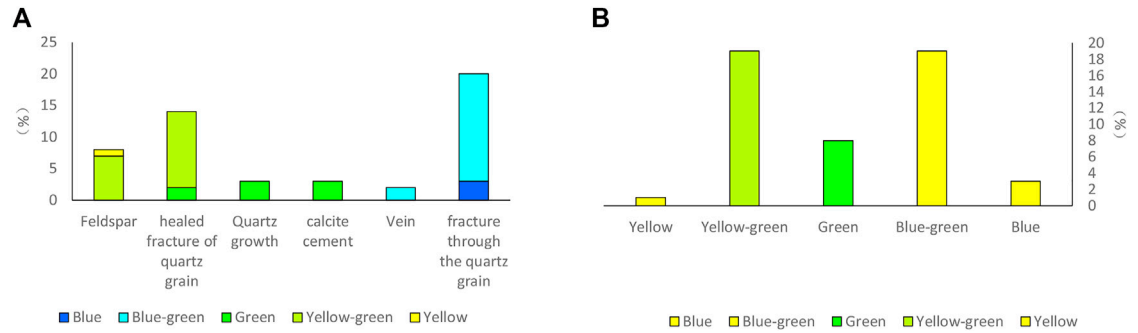

FIGURE 3 | (A) Histogram of oil inclusions in various diagenetic minerals. **(B)**: Histogram of numbers of oil inclusions with various colors.

composition and evolution degree of oil inclusions (Munz, 2001; Su et al., 2020).

(Explanation: Microscopic fluorescence spectrum parameters of a single oil inclusion (Q value, λ_{max}, and QF_{535}) is one of the effective methods to evaluate the maturity and oil charging multistage of oil inclusions, and it is defined as follows: The definition of the red and green quotient Q value: Q value = I_{650}/I_{500}, where I_{650} is the fluorescence intensity corresponding to a spectral wavelength of 650 nm, and I_{500} is the fluorescence intensity corresponding to a spectral wavelength of 500 nm. The I_{650} value mainly reflects the information of the macromolecular components in the inclusion oil with lower maturity. The larger the I_{650} value, the more the macromolecular components contained in the inclusion oil. The I_{500} value mainly reflects the information of the small molecular components in the inclusion oil with higher maturity. The larger the I_{500} value, the smaller the molecule components contained in the inclusion oil. Therefore, the greater the red–green quotient (Q), the lower the maturity of the oil in the inclusions, and vice versa. λ_{max} is the wavelength corresponding to the main peak of the microbeam fluorescence spectrum of oil inclusions. The larger the λ_{max}, the lower the maturity. The smaller the λ_{max}, the higher the maturity. The relationship between Q and λ_{max} well reflects the maturity of oil inclusions. QF_{535} is defined as the ratio of the area defined by the wavelength of 720 and 535 nm to the area defined by the wavelength of 535 and 420 nm. The larger the QF_{535}, the higher the content of high molecular weight hydrocarbon components and the lower the oil maturity of the inclusion.)

The microscopic observation of thin sections of fluid inclusion in the study area shows that the inclusions in the FGSR reservoir mainly consist of pure oil single-phase inclusions, gas–liquid two-phase oil inclusions, pure water liquid-phase inclusions, two-phase hydrocarbon-bearing inclusions, and bitumen inclusions. Inclusions have varied shapes, mainly oval, followed by strip-shaped and nearly circular. The size range of the inclusions is 3–7 μm. Oil fluid inclusions show rich microscopic oil and gas. Oil inclusions with different fluorescent colors are distributed in a variety of occurrences including feldspar (**Figures 2A,B**), cracks in quartz grains (**Figures 2C,D**), quartz overgrowth (**Figures 2E,F**), calcite cements (**Figures 2G,H**), veins, and cracks through quartz particles (**Figures 2I,J**), accounting for 16, 28, 6, 6, 4, and 40%, respectively (**Table 1**; **Figure 3A**).

The fluorescence spectrum characteristics and the spectral parameters (**Table 1**) of the inclusions in the FGSR reservoir in the study area show that the fluorescence colors of hydrocarbon inclusions are yellow, yellow–green, green, blue–green, and bright blue, accounting for 2, 38, 16, 38, and 6%, respectively (**Figure 3B**). There are obvious differences in the spectra of oil inclusions of different fluorescent colors, reflecting the maturity difference of oil inclusions. The λ_{max} of low-maturity yellow fluorescent oil inclusions is 582.25 nm, and QF535 is 2.85. The λ_{max} of mature yellow–green and green fluorescent oil inclusions is 502–548 nm, and QF535 is 0.86–1.86. The λ_{max} of highly mature bright blue and blue–green fluorescent oil inclusions is 463–499 nm, and QF535 is 0.64–1.325 (Wu et al., 2018). It can be seen that the FGSR reservoir in the study area generally has three stages of oil sources: low-mature, mature, and high-mature, of which mature–high-mature oil charging is the main oil source supply.

Microscopic Temperature Measurement Analysis of Hydrocarbon Inclusions

Based on the identification and analysis of the fluorescence characteristics of oil inclusions, the homogenization temperature of different occurrences, different types of oil inclusions, and their symbiotic brine inclusions were further measured. The homogenization temperature of the brine inclusions coexisting with hydrocarbon inclusions was measured. In the data collation, the inclusions with a temperature difference greater than 20°C in the same occurrence were excluded. Based on the fluorescence observation of oil inclusions, the representative samples were subjected to microscopic temperature measurement and salinity measurement analysis, and the following data were obtained. The homogenization temperature range and mean salinity of brine inclusions in the first phase is 115.1–123.4°C and 21.9 wt.% NaCl, respectively; in the second phase, they are 14.5–146.7°C and 16.5 wt.% NaCl; and in the third phase, they are 148.5–160.4°C and 8.8 wt.% NaCl. The homogenization temperature of oil inclusions is relatively wide, mainly distributed in four temperature ranges: in

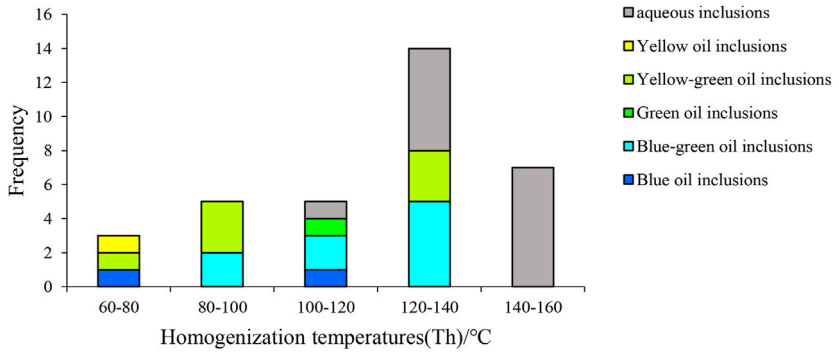

FIGURE 4 | Histograms of homogenization temperatures for oil inclusions with various colors and coeval aqueous inclusions in the FGSR reservoir.

the first phase, 68.1–75.9°C; in the second phase, 82.8–99.6°C; in the third phase, 101.8–121.2°C; and in the fourth phase, 148.5–160.4°C (**Figure 4**).

DISCUSSION

The densification process of the FGSR reservoir of the Chang 7 Member of the Triassic Yanchang Formation in the Zhenyuan area of the southwest Ordos Basin has experienced a long period of geological history, accompanied by the generation and migration of oil. The discussion of the diagenetic evolution process of the FGSR reservoir and how the oil charging affects the densification process of the reservoir has important guiding value for predicting the scale of tight oil accumulation.

Diagenesis and Diagenetic Evolution Characteristics

FGSRs have undergone a series of diagenetic evolutions from the initial loose sedimentary state until metamorphism, and the most direct result is the continuous reduction of reservoir pores and gradual densification (Li et al., 2021). Combined with the comprehensive analysis of fluid inclusions, scanning electron microscopy, cathodoluminescence, and cast thin sections, the FGSRs of the Chang 7 Member of the Triassic Yanchang Formation in the Zhenyuan area have undergone complex diagenetic evolution processes including compaction, cementation, and multiple dissolutions.

Compaction was the earliest continuous diagenesis after the deposition of FGSRs, and it almost accompanied the entire process of FGSR evolution (Liu et al., 2020). The FGSR reservoir of the Chang 7 Member in the study area had typical compaction. Observations under microscope and scanning electron microscope show that the directional arrangement of the particles, the line contact–concave–convex contact between the particles, and the large number of primary intergranular pores were destroyed, leaving relatively few residual pores (**Figure 5A**). The phyllite, schist, slate, mica (**Figures 5B,C**), and other plastic components in the cuttings have weaker compaction resistance. Compared with rocks with high quartz content, they are prone to plastic deformation. Strong compaction is the main reason why the physical properties of the reservoir were deteriorated (Beard and Weyl, 1973).

Cementation is the crystallization and precipitation of the supersaturated components of the solution in the pores, resulting in further consolidation of loose sediments, which is a key factor leading to further densification process of the reservoir. Cementation was generally developed in the FGSR reservoir of the Chang 7 Member in the study area, mainly including ferrocalcite cement (**Figure 5D**), calcite, chlorite (**Figures 5E,G, I**), quartz overgrowth (**Figure 5G**), kaolinite (**Figure 5E**), illite (**Figure 5H**), iron calcite, and other minerals. The higher feldspar content in the FGSRs of the Chang 7 Member in the study area provided the material basis for the formation of illite during the diagenetic evolution. With the increase of illite content, the porosity and permeability of sandstone showed a decreasing trend (Fu et al., 2013). The iron calcite cement was a product formed at a relatively late stage of diagenesis. Its massive formation not only made the physical properties of the reservoir worse, but also was an important factor that caused strong heterogeneity.

Compared with cementation, dissolution has a constructive effect on reservoirs. The further selective dissolution of original minerals and cements is the most important factor for increasing porosity and permeability. The FGSRs of the Chang 7 Member of the Zhenyuan area were mainly feldspar lithic sandstone and lithic feldspar sandstone, which had low component maturity and provided innate conditions for dissolution. The acidic water released during the hydrocarbon generation stage of organic matter and the organic acids in oil charging accelerated dissolution (Zhu et al., 2014; Zhu et al., 2015). The internal and inter-particle dissolutions were developed, including feldspar dissolution (**Figures 5F, J, K**) and quartz dissolution, forming a large number of secondary dissolution pores (**Figures 5I,L**).

According to China Oil & Gas Industry Standards and the characterization of the diagenetic evolution sequence of clay minerals, combined with Ro, oil inclusion temperature analysis, and a comprehensive analysis of diagenesis characteristics, we find that the Yanchang Formation sandstone in the Ordos Basin as a whole is currently in the A2 period of mid-diagenesis stage, part of it is in the B period of

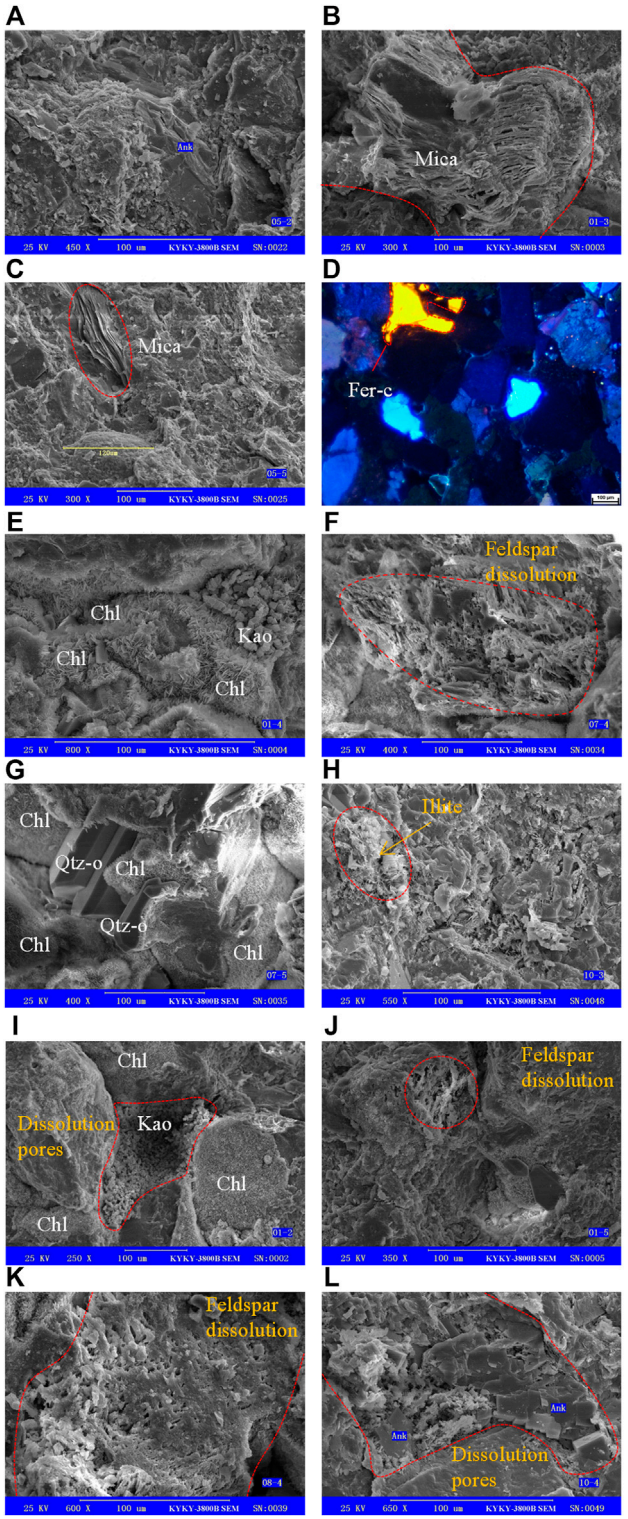

FIGURE 5 | SEM image and cathodoluminescence (CL) image showing the optical characteristics of diagenesis in the FGSR reservoir. **(A)** Sample 2461.5 m, well Z156: primary pores were destroyed by mechanical compaction. **(B)** Sample 2384 m, well Y72: mica was deformed by mechanical compaction. **(C)** Sample 2461.5 m, well Z156: mica was deformed by mechanical compaction. **(D)** Sample 2492.5 m, well Y108: ferrocalcite cement (Fer-c). **(E)** Sample 2384 m, well Y72: the chlorite (Chl) and kaolinite (Kao). **(F)** Sample 2692.07 m, well Z106: feldspar dissolution. **(G)** Sample 2692.07 m, well Z106: quartz overgrowth (Qtz-o) and chlorite (Chl). **(H)** Sample 2066m, well Z221: fibrous illite. **(I)** Sample 2384 m, well Y72: the dissolution pores was filled in by kaolinite (Kao), and surrounded by chlorite (Chl). **(J)** Sample 2384 m, well Y72: feldspar dissolution. **(K)** Sample 2360.5 m, well Y75: feldspar dissolution. **(L)** Sample 2066 m, well Z221: dissolution pores.

mid-diagenesis stage, and that the average porosity of the reservoir is about 10%; the total porosity is basically stable, and the overall reservoir is tight (**Figure 6**).

Coupling Relationship Between Reservoir Densification and Accumulation

The densification process of the FGSR reservoir has started from the quasi-contemporaneous stage, accompanied by the continuous process of the entire diagenetic evolution as well as the process of oil charging at different stages.

Different types of oil have a close relationship with diagenesis. Yellow and yellow–green oil inclusions are mainly seen in feldspar, indicating low-mature oil and mature oil charging, respectively; yellow–green and green oil inclusions are mainly seen in the cracks in quartz grains, indicating mature oil charging; green oil inclusions are mainly seen in quartz overgrowth and calcite cements, indicating mature oil charging; blue–green and bright blue oil inclusions are mainly seen in veins and cracks through quartz grains, indicating high-mature oil charging (**Figure 7**). Different types of oil charging reflect different diagenetic sequences: the formation of feldspar pores is earlier, followed by cracks in quartz grains, quartz overgrowth, calcite cements, and finally cracks through quartz grains.

The FGSR reservoir particles in the study area are in very close contact with small pore spaces. Normally, oil is still stored when pore throat diameters are less than 1 μm. To a certain extent, it reflects that there was sufficient hydrocarbon expulsion pressure during the geological history period (Wu et al., 2016). It also shows that in the oil charging stage, the FGSR reservoir had good storage capacity and has not yet reached the degree of densification of tight reservoirs.

The diagenetic system composed of FGSRs and fluids is an open and semi-open system. The pressure difference in the diagenesis process and the newly added storage space make it easier for oil charging. The formation of fluid inclusions is accompanied by oil migration and accumulation. Using the homogenization temperature of the brine inclusions in the same period as the hydrocarbon inclusions, combined with the paleotemperature history and reservoir burial history in the study area, the formation time of tight oil reservoirs can be determined to further analyze the spatiotemporal coupling relationship between reservoir densification and accumulation time.

Then, the burial history projection method was used to determine the oil charging time. The analysis shows that the corresponding geological times of the three phases of oil charging are: in the first phase, the charging time is 132–124 Ma, in the

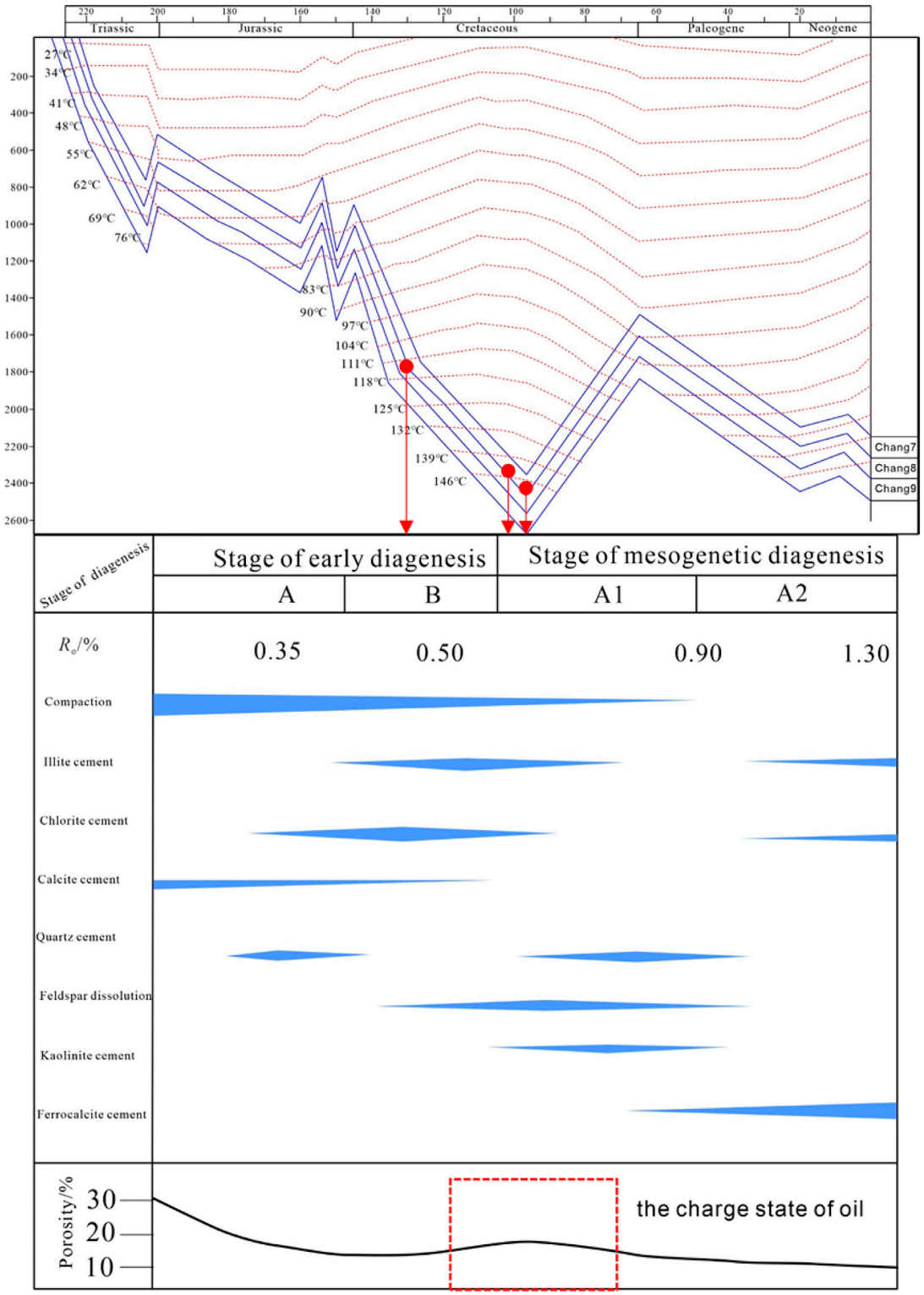

FIGURE 6 | Burial-thermal history, diagenetic sequences, and the evolution of pores in the FGSR reservoir.

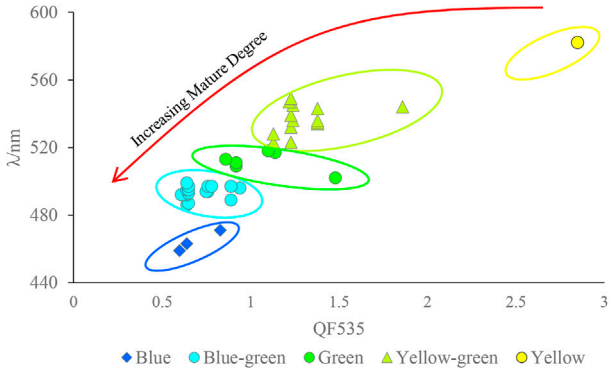

FIGURE 7 | Cross-plot of QF535 and λmax values for single oil inclusions in the FGSR reservoir.

second phase 120–102 Ma, and in the third phase 98–97 Ma (**Figure 6**).

It can be seen from **Figure 6** that during the first charging phase (132–124 Ma), the burial depth of the formation gradually increased, and with the enhancement of compaction, the intergranular pores of the reservoir decreased. The discovery of low-mature oil marked by yellow fluorescent inclusions in feldspar dissolution pores indicates that oil charging was closely related to the dissolution of feldspar. The study area is close to the hydrocarbon generation center, and the Chang 7 Member itself is a high-quality reservoir with source rocks. During the maturation of source rocks, a large number of acidic fluids were continuously discharged, and the feldspar and cuttings of adjacent reservoirs were dissolved and transformed (Zhu et al., 2014; Zhu et al., 2015; Zhang et al., 2020). Before the early low-mature oil charging, certain feldspar dissolved pores had developed in the FGSR reservoir, which increased the storage space with the continuous increase in compaction. With the early charging of low-mature oil, organic matter expulsion of hydrocarbons released organic acids into the FGSR reservoir, and further dissolution occurred with soluble materials such as feldspar and cuttings, which effectively improved the physical properties of the reservoir and provided effective storage space for the next large-scale oil charging, while the disadvantage is that it also provided a sedimentation space for the formation of cement.

In the second charging phase (120–102 Ma), as the burial depth continued to increase, the maturity of organic matter increased. When the organic acid produced by the low-mature oil accelerated the dissolution and increased the storage capacity of the FGSR reservoir, the number of yellow–green oil inclusions in the feldspar dissolution pores has increased significantly. Then, the oil charging has entered the peak stage, producing a large number of organic acids, and increasing the probability of dissolution of feldspar and cuttings. At the same time, the abnormal high pressure generated by oil charging inhibited the destructive effect of compaction on the FGSR reservoir to a certain extent (Wu et al., 2016). On the other hand, with the increase in the degree of thermal evolution of organic matter, yellow–green and green inclusions appeared in the cracks in quartz grains, quartz overgrowth, and calcite cements, reflecting that a large number of cements were formed before mature oil charging.

In the third charging phase (98–97 Ma), the burial depth increased rapidly, the maximum burial depth of source rocks reached the maximum, and the oil generation rate was the highest. The Chang 7 source rocks entered the peak of hydrocarbon generation. While the large-scale high-maturity oil was charged, the acidification of large-scale organic acids played a constructive role in the formation of secondary pores. At the same time, as the depth increased, chlorite is more and more developed (**Figure 8A**), and a large number of pores were covered by chlorite (**Figure 8B**). On the contrary, the content of kaolin decreased, reducing the probability of clay minerals filling secondary pores. The preservation of pores (Xie et al., 2010; Zhu et al., 2014) increased pore connectivity, and provided favorable conditions for oil charging in the third phase.

After continuous diagenetic reformation and intermittent oil charging, the FGSR reservoir has experienced a cyclical reservoir densification process of "reducing porosity-increasing porosity-preserving porosity". The coupling of overall densification process of the reservoir, pore increase at different stages, regional pore preservation, and oil charging is the key to the extensive accumulation and large-scale reservoir formation of tight oil in the Chang 7 Member of the Yanchang Formation in the Zhenyuan area, southwest Ordos Basin.

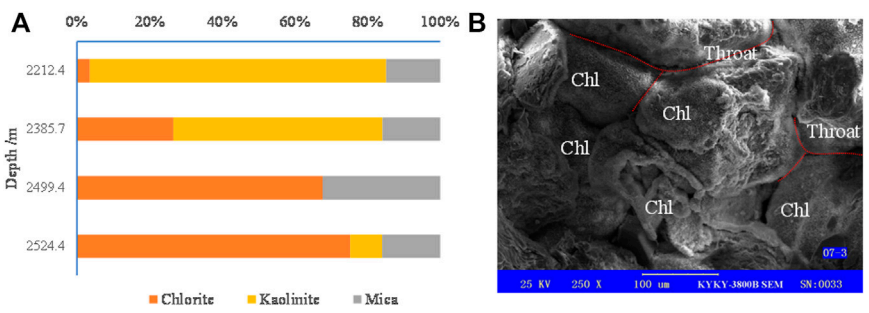

FIGURE 8 | (A) Histogram of mineral content as depth increases. **(B)** SEM image showing the optical characteristics of chlorite which protect the pores.

CONCLUSION

This research mainly studied the fluid inclusions and diagenesis of the Chang 7 Member FGSR reservoir of the Yanchang Formation in the Zhenyuan area of the southwest Ordos Basin, and discussed the relationship between reservoir densification characteristics and tight oil accumulation. The following conclusions can be drawn:

1) The FGSR reservoir inclusions are mainly distributed in feldspar, cracks in quartz grains, quartz overgrowth, calcite cements, and veins and cracks through quartz grains. The fluorescence colors of oil inclusions include yellow, yellow–green, green, blue–green, and bright blue. There are three stages of oil source charging of low-maturity, maturity, and high-maturity, corresponding to three different geological historical periods.
2) The FGSR reservoir has undergone long-term and complex diagenesis transformations such as compaction, cementation, and dissolution, and the process of gradual densification process was accompanied by oil charging. The first phase of small-scale oil charging provided organic acids, which promoted dissolution, increased secondary pores, and provided storage space for the next phase of oil charging; the oil charging in the second phase increased significantly, resulting in organic acid that promoted the dissolution of feldspar and cuttings, and increased the pores; in the third stage of oil charging, the stratum burial depth reached the maximum, the compaction effect was the strongest, and the organic acid promoted the formation of secondary pores, while the chlorite membrane protected pores from those that were filled or compacted, increasing connectivity.
3) The three stages of oil charging and FGSR reservoir densification process were coordinated and accompanied by time–space coupling, and have experienced "reduced porosity-increased porosity-porosity preservation" multi-phase reservoir densification and oil accumulation at different stages, jointly leading to the large-scale tight oil accumulation in the study area. This study may help to understand the process of the tight oil accumulation, and predict the tight oil of the FGSR reservoir distribution of the Yanchang Formation in the Zhenyuan area of the southwest Ordos Basin, central China.

DATA AVAILABILITY STATEMENT

The original contributions presented in the study are included in the article/supplementary material. Further inquiries can be directed to the corresponding author.

AUTHOR CONTRIBUTIONS

WH: conceptualization, resources, methodology, formal analysis, resources, writing—original draft, writing—review, and editing; RW: methodology, investigation, formal analysis, supervision, editing, and revision; QL: conceptualization, methodology, supervision, and funding acquisition; JL: methodology and resources; and YW: conceptualization and methodology. All authors reviewed the article.

FUNDING

This study was financially supported by the Foundation of State Key Laboratory of Shale Oil and Gas Enrichment Mechanisms and Effective Development (No. GSYKY-B09-33) at SINOPEC Petroleum Exploration and Production Research Institute, National Natural Science Foundation of China (No. 42102170), and SINOPEC Ministry of Science and Technology Project (Grant No. P21026). SINOPEC was not involved in the study design, collection, analysis, interpretation of data, the writing of this article or the decision to submit it for publication.

REFERENCES

Beard, D. C., and Weyl, P. K. (1973). Influence of Texture on Porosity and Permeability of Unconsolidated Sand. *AAPG Bull.* 57, 349–369. doi:10.1306/819A4272-16C5-11D7-8645000102C1865D

Cui, L. T., Hao, S., Wang, C. P., Zhu, W. T., et al. (2015). Palaeogeomorphology Reconstruction and Sandbody Distributionof the Chang 7-6 Intervals of Triassic Yanchang Formationin Northern Zhenyuan Area, Ordos Basin. *J. Palaeogeogr. (Chinese Edition)* 17 (6), 805–812.

Deng, X. Q., Luo, X. S., and Liu, X. S. (2009). The Relationship between Compacting History and Hydrocarbon Accumulating History of the Super-low Permeability Reservoirs in the Triassic Yanchang Formation in the Ordos Basin. *Oil Gas Geology.* 30 (2), 156–161. doi:10.11743/ogg20090205

Fu, G. X., Zhao, J. X., Zhang, Z. S., Meng, H. F., and Song, J. W. (2010). The Provenance and Features of Depositional System in the Yanchang Formation of Triassic in Southeast Area of Ordos Basin. *Mineralogy Pet.* 30 (1), 99–105. doi:10.3969/j.issn.1001-6872.2010.01.016

Fu, J., Wu, S. H., Luo, A. X., Zhang, L. A., Li, Z., and Li, J. H. (2013). Reservoir Quality and its Controlling Factors of Chang 8 and Chang 6 Members in Longdong Area, Ordos Basin. *Earth Sci. Front.* 20 (2), 98–107.

Guo, J. G., Guo, K., Gong, P. Q., Xv, J., Guo, J., et al. (2017). Reservoir Densification and Tight-Oil Charging in Yanchang Formation, Ordos Basin. *Pet. Geology. Exp.* 39 (2), 169–179. doi:10.11781/sysydz201702169

Huang, S., Wu, Y., Meng, X., Liu, L., and Ji, W. (2018). Recent Advances on Microscopic Pore Characteristics of Low Permeability Sandstone Reservoirs. *Adv. Geo-energy Res.* 2 (2), 122–134. doi:10.26804/ager.2018.02.02

Li, B., Zhang, H., Xia, Q., Peng, J., and Guo, Q. (2021). Quantitative Evaluation of Tight Sandstone Reservoir Based on Diagenetic Facies-A Case of Lower Silurian Kepingtage Formation in Shuntuoguole Low Uplift, Tarim Basin, China. *Front. Earth Sci.* 8, 597535. doi:10.3389/feart.2020.597535

Li, D. H., Liu, Z. Y., Zhang, G. S., Zheng, Z. H., Jia, J., Gao, X., et al. (2017). Comparison and Revelation of Tight Oil Accumulation Conditions, Distribution Characteristics and Development Status between China and U.S. *Nat. Gas Geosci.* 28 (7), 1126–1138. doi:10.11764/j.issn.1672-1926.2017.07.004

Li, X. B., Yang, Z. L., Wang, J., Liu, H. Q., Chen, Q. L., Wanyan, R., et al. (2016). Mud-coated Intraclasts: a Criterion for Recognizing Sandy Mass-Transport Deposits-Deep-Lacustrine Massive Sandstone of the Upper Triassic Yanchang Formation, Ordos Basin, Central China. *J. Asian Earth Sci.* 103 (2), 98–116. doi:10.1016/j.jseaes.2016.06.007

Liao, J. J., Zhu, X. M., Deng, X. Q., Sun, B., Hui, X., et al. (2013). Sedimentary Characteristics and Model of Gravity Flow in Triassic Yanchang Formation of Longdong Area in Ordos Basin. *Earth Sci. Front.* 20 (2), 29–39.

Liu, Y., Xian, C., Li, Z., Wang, J., and Ren, F. (2020). A New Classification System of Lithic-Rich Tight sandstone and its Application to Diagnosis High-Quality Reservoirs. *Adv. Geo-energy Res.* 4 (3), 286–295. doi:10.46690/ager.2020.03.06

Loucks, R. G., Reed, R. M., Ruppel, S. C., and Jarvie, D. M. (2009). Morphology, Genesis, and Distribution of Nanometer-Scale Pores in Siliceous Mudstones of the Mississippian Barnett Shale. *J. Sediment. Res.* 79 (12), 848–861. doi:10.2110/jsr.2009.092

Munz, I. A. (2001). Petroleum Inclusions in Sedimentary Basins: Systematics. *Anal. Methods Applications" Lithos* 55 (1), 195–212. doi:10.1016/s0024-4937(00)00045-1

Ran, X. Q., Wu, S. H., Fu, J., Wei, X. S., Chu, M. J., et al. (2013). Research on the Pore Structure Classification of Low Permeability Reservior of theYanchang Formation in Longdong Area,Ordos Basin. *Earth Sci. Front.* 20 (2), 77–85.

Sonnenberg, S. A., and Pramudito, A. (2009). Petroleum Geology of the Giant Elm Coulee Field, Williston Basin. *Bulletin* 93 (9), 1127–1153. doi:10.1306/05280909006

Su, A., Chen, H. H., Zhao, J. X., and Feng, Y. X. (2020). Integrated Fluid Inclusion Analysis and Petrography Constraints on the Petroleum System Evolution of the Central and Southern Biyang Sag, Nanxiang Basin, Eastern China. *Mar. Pet. Geology.* 118, 104437. doi:10.1016/j.marpetgeo.2020.104437

Wang, R., Hu, Z., Zhou, T., Bao, H. Y., Wu, J., Du, W., et al. (2021). Characteristics of Fractures and Their Significance for Reservoirs in Wufeng-Longmaxi Shale, Sichuan Basin and its Periphery. *Oil Gas Geology.* 42 (6), 1295–1306. (in Chinese). doi:10.11743/ogg20210605

Wang, R. Y., Hu, Z. Q., Long, S. X., Liu, G. X., Zhao, J. H., Du, W., et al. (2019). Differential Characteristics of the Upper Ordovician-Lower Silurian Wufeng-Longmaxi Shale Reservoir and its Implications for Exploration and Development of Shale Gas In/around the Sichuan Basin. *Acta Geologica Sinica - English Edition* 93 (3), 520–535. doi:10.1111/1755-6724.13875

Wang, R. Y., Nie, H. K., Hu, Z. Q., Liu, G. X., Xi, B. B., and Liu, W. X. (2020). Controlling Effect of Pressure Evolution on Shale Gas Reservoirs: A Case Study of the Wufeng–Longmaxi Formation in the Sichuan Basin[J]. *Nat. Gas Industry* 40 (10), 1–11. doi:10.3787/j.issn.1000-0976.2020.10.001

Wu, K. J., Liu, L. F., Xv, Z. J., Dou, W. C., Luo, A. X., Fu, J. H., et al. (2016). Lower Limits of Pore Throat Radius, Porosity and Permeability for Tight Oil Accumulations in the Chang7 Member, Ordos Basin. *Pet. Geology. Exp.* 38 (1), 63–69.

Wu, W. T., Deng, J., Zhao, J. Z., Sun, B., Guo, H. Q., Deng, X. Q., et al. (2016). Accumulation Conditions and Models of Tight Oil Reservoirs in Chang-7 of Huaqing Area, the Ordos Basin. *OIL GAS GEOLOGY.* 37 (6), 874–881. doi:10.11743/ogg20160609

Wu, Y., Wang, H. H., Luo, S. S., Lyu, Q. Q., Li, L. D., He, W. L., et al. (2018). Differential Hydrocarbon Charging History of Chang 8 Tight Sandstone Reservoir of Yanchang Formation in Zhenyuan Area,Ordos Basin. *Bull. Geol. Sci. Tech.* 37 (1), 153–159.

Xie, W. R., Yang, W., Zhao, X. Y., Wei, G. Q., Xie, Z. Y., Jin, H., et al. (2010). Influences of Chlorite on Reservoir Physical Properties oftheXujiahe Formation in the central Part of Sichuan Basin. *Pet. Exploration Dev.* 37 (6), 674–679.

Yang, H., Dou, W. T., Liu, X. Y., and Zhang, C. L. (2010). Analysis on Sedimentary Facies of Member7 in Yanchang Formation of Triassic in Ordos Basin. *Acta Sedimentologica Sinica* 28 (2), 254–263.

Yang, H., Liang, X. W., Niu, X. B., Feng, S. B., and You, Y. (2017). Geological Conditions for continental Tight Oil Formation and the Main Controlling Factors for the Enrichment: A Case of Chang 7 Member, Triassic Yanchang Formation, Ordos Basin, NW China. *Pet. Exploration Dev.* 44 (1), 12–20. doi:10.11698/ped.2017.01.02

Yang, R. C., Fan, A. P., Han, Z. Z., and Van Loon, A. J. (2017). Lithofacies and Origin of the Late Triassic Muddy Gravity-Flow Deposits in the Ordos Basin, Central China. *Mar. Pet. Geology.* 3, 194–219. doi:10.1016/j.marpetgeo.2017.05.005

Yang, R. C., Jin, Z. J., Van Loon, A. J., Han, Z. Z., and Fan, A. P. (2019). Climatic and Tectonic Controls of Lacustrine Hyperpycnite Origination in the Late Triassic Ordos Basin, Central China: Implications for Unconventional Petroleum Development: Reply. *AAPG Bull.* 103 (2), 511–514. doi:10.1306/08151818057

Yao, J. L., Deng, X. J., Zhao, Y. D., Han, T. Y., Chu, M. J., and Pang, J. (2013). Characteristics of Tight Oil in Triassic Yanchang Formation, Ordos Basin. *Pet. Exploration Dev.* 40 (2), 150–158. doi:10.1016/s1876-3804(13)60019-1

Yuan, X. J., Lin, S. H., Liu, Q., Yao, J. L., Wang, L., Guo, H., et al. (2015). Lacustrine fine-grained Sedimentary Features and Organic-Rich Shale Distribution Pattern: A Case Study of Chang 7 Member of Triassic Yanchang Formation in Ordos Basin, NW China. *Pet. Exploration Dev.* 42 (1), 34–43. doi:10.1016/S1876-3804(15)60004-0

Zhang, K., Jiang, S., Zhao, R., Wang, P., Jia, C., and Song, Y. (2022). Connectivity of Organic Matter Pores in the Lower Silurian Longmaxi Formation Shale, Sichuan Basin, Southern China: Analyses from Helium Ion Microscope and Focused Ion Beam Scanning Electron Microscope. *Geol. J.*, 1–13. doi:10.1002/gj.4387

Zhang, K., Peng, J., Wang, X., Jiang, Z., Song, Y., Jiang, L., et al. (2020). Effect of Organic Maturity on Shale Gas Genesis and Pores Development: A Case Study on marine Shale in the Upper Yangtze Region, South China. *Open Geosciences* 12, 1617–1629. doi:10.1515/geo-2020-0216

Zhang, Z. J., Chen, S. Y., Xiao, Y., Lu, J. G., Yang, G. P., Tang, H. P., et al. (2013). Characteristics of the Chang 8 Tight sandstone Reservoirs and Their Genesis in Huaqing Area, Ordos Basin. *Oil Gas Geology.* 34 (5), 679–684. doi:10.11743/ogg20130515

Zhao, Y., Wang, Y. B., Zhong, D. K., Xv, Q., Zhao, X., Huo, C., et al. (2018). Study on the relationship between tight sandstone reservoir Diagenetic Evolution and Hydrocarbon Reser-Voirs Filling: A Case from the Yanchang Formation, Ordos Basin. *J. Mining Sci. Tech.* 3 (2), 106–118.

Zhu, H. H., Zhong, D. K., Yao, J. L., Niu, X. B., Liang, X. W., Zhao, Y., et al. (2014). Microscopic Characteristics and Formation Mechanism of Upper Triassic Chang 7tight Oil Reservoir in the Southwest Ordos Basin. *J. China Univ. Mining Tech.* 43 (5), 853–863. doi:10.13247/j.cnki.jcumt.000095

Zhu, H. H., Zhong, D. K., Yao, J. L., Sun, H. T., Niu, X. B., Liang, X. W., et al. (2015). Alkaline Diagenesis and its Effects on Reservoir Porosity: A Case Study of Upper Triassic Chang 7 Tight Sandstones in Ordos Basin, NW China. *Pet. Exploration Dev.* 42 (1), 51–59. doi:10.11698/ped.2015.01.06

Zou, C. N., Wang, L., Li, Y., Tao, S. Z., and Hou, L. H. (2012). Deep-lacustrine Transformation of Sandy Debrites into Turbidites, Upper Triassic, Central China. *Sediment. Geology.* X, 143–155. doi:10.1016/j.sedgeo.2012.04.004

Conflict of Interest: Authors WH and RW were employed by the company China Petroleum and Chemical Corporation (SINOPEC). JL was employed by PetroChina Changqing Oilfield Company.

The remaining authors declare that the research was conducted without any commercial or financial relationships that could be construed as a potential conflict of interest.